A Neutron Scattering and Nuclear Magnetic Resonance Study of the Structure of $GeO_2-P_2O_5$ Glasses

J. W. Zwanziger,*,† J. L. Shaw,† U. Werner-Zwanziger,† and B. G. Aitken‡

Department of Chemistry and Institute for Research in Materials, Dalhousie University, Halifax, NS, Canada, and SP-FR-05, Corning Inc., Corning, New York 14831

Received: April 20, 2006; In Final Form: June 20, 2006

Germanophosphate ($GeO_2-P_2O_5$) glasses were studied with neutron diffraction, phosphorus, and oxygen nuclear magnetic resonance, calorimetry, viscosity measurements, and first-principles calculations. These data sets were combined to propose a structural model of $GeO_2-P_2O_5$ glasses, which includes tetrahedrally coordinated phosphorus, formation of octahedrally coordinated germanium as P_2O_5 content increases, an absence of trigonally coordinated oxygen, and hence an absence of rutile-like GeO_2 domains. The structural model was then used to propose explanations for both the observed composition dependence of the glass transition temperature and the fragility of the $GeO_2-P_2O_5$ liquids.

1. Introduction

Germanophosphate ($GeO_2-P_2O_5$) glasses can be regarded as base materials in some technologically important systems. For example, fast lithium ion conducting glass ceramics, which are potential electrolyte materials for high energy density batteries, can be obtained by heat treatment of $Li_2O-Al_2O_3-GeO_2-P_2O_5$ glasses.[1] There are efforts to use germanate glasses instead of silica in optical fiber technology because of their superior transparency in the midinfrared region,[2] but progress is hampered by their high Rayleigh scattering loss. In silica glass, scattering loss can be reduced initially by alloying with P_2O_5, which lowers the glass transition temperature (T_g). However, a similar addition of P_2O_5 to GeO_2, in the 5−20 mol % P_2O_5 regime, *increases* T_g (after an initial decrease upon going from 0% P_2O_5 to 5% P_2O_5), thereby increasing the scattering loss. This effect on T_g is believed to be due to an increase in the coordination of some Ge atoms from 4 to 6,[3] although in silica, addition of P_2O_5 does not cause a similar change in the coordination of Si.[4] In another important oxide, Al_2O_3, addition of P_2O_5 seems to force some of the 6-fold coordinated Al atoms into 4-fold coordination.[5] Thus, we have a puzzling array of data on the influence of P_2O_5 on the coordination of network forming cations in oxides. Furthermore, we recently undertook structural investigations on $GeS_2-P_2S_5$ glasses, which can be considered as covalent analogues of $GeO_2-P_2O_5$, and found that Ge retained 4-fold coordination for all compositions.[6,7] By replacing sulfur with the more electronegative oxygen, we are also in a position to understand the role of ionicity in the larger $GeX_2-P_2X_5$ system. Together, these various facts clearly illustrate that a comprehensive investigation of $GeO_2-P_2O_5$ glass is of fundamental significance. However, there are only a few reported studies of this as a pure binary system.[3,8] Here, neutron scattering and NMR techniques are combined with glass transition temperature (T_g) and viscosity (η) data to probe the structure of the germanophosphate system.

Two crystalline polymorphs of GeO_2 exist, having the rutile or quartz structure. The quartz structure contains only 4-fold coordinated germanium atoms (Ge^{IV}) in GeO_4 tetrahedra, linked by two-coordinate oxygen, whereas the germanium in the rutile form is 6-fold coordinated (Ge^{VI}), in GeO_6 octahedra linked by three-coordinate oxygen. These structures are shown in Figure 1. Pure vitreous GeO_2 consists of corner-sharing GeO_4 tetrahedra connected in a continuous random network, similar to the quartz structure.[9] Network modifying cations added to the matrix can induce a change in the coordination number of some of the germanium atoms from 4 to 6,[10] similar to what is seen in silicophosphates.[11] Part of the aim of this paper is to confirm if, and to what degree, phosphorus ions of the network forming oxide, P_2O_5, have the same effect.

The PO_4 tetrahedron, with varying numbers of bridging oxygen atoms (BO), is the basic structural unit in all phosphate glasses. The standard nomenclature is Q^n, where n denotes the number of bridging oxygen connected to the unit. In amorphous P_2O_5, all phosphorus are of Q^3 type, with each sharing corners to three adjacent PO_4 tetrahedra, while the fourth oxygen is neutral and nonbridging, and is linked to the phosphorus through a double bond. When ionic modifiers are added to P_2O_5, bridging oxygen bonds are cleaved and $Q^{2,1,0}$ species are formed. On the other hand, when a covalent component is added, such as GeO_2 in the present case, it would be expected that either the same Q^3 species would be maintained, or possibly Q^4 tetrahedra, with four equivalent bridging bonds, would be formed, or finally an intermediate structure that is four-coordinate but with asymmetric bonding. Such possible phosphate units are shown in Figure 1.

2. Experimental Details

2.1. Samples. Germanium phosphate glasses, $(GeO_2)_x(P_2O_5)_{100-x}$ (x in mol %), were made at five compositions containing 5, 10, 15, 20, and 25 mol % P_2O_5. These are labeled here as P5, P10, P15, P20, and P25, respectively, for ease of notation. The samples were made at Corning Inc. by a two-step process to minimize P_2O_5 volatility problems. A base glass was prepared from 289 g of GeO_2 and 343 g of H_3PO_4, which, due to P_2O_5 volatility, resulted in a glass with a composition of 30 mol % P_2O_5. This glass was made by blending GeO_2 and H_3PO_4 in a platinum crucible to form an homogeneous slurry.

* To whom correspondence should be addressed. E-mail: jzwanzig@dal.ca.
† Dalhousie University.
‡ Corning, Inc.

10.1021/jp062432n CCC: $33.50
Published on Web 09/15/2006

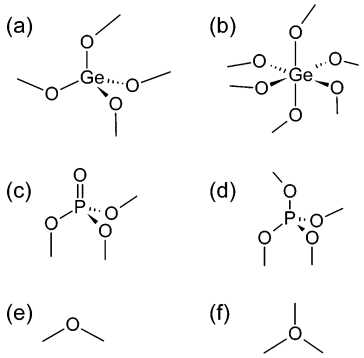

Figure 1. Structural units considered in the analysis of $GeO_2-P_2O_5$ glasses: (a) GeO_4 tetrahedron, as found in quartz-structured GeO_2; (b) GeO_6 octahedron, as found in GeP_2O_7 and rutile-structured GeO_2; (c) conventional Q^3 phosphate; (d) four-coordinate phosphate as found in $Ge_5O(PO_4)_6$ and GeP_2O_7; (e) two-coordinate oxygen as found in most corner-sharing oxide glasses; (f) three-coordinate oxygen as found in rutile-structured GeO_2.

TABLE 1: $GeO_2-P_2O_5$ Glass Samples (Nominal and Actual) Used in This Study, along with Mass Densities and Derived Molar Volume

	nominal mol %		actual mol %			
sample	GeO_2	P_2O_5	GeO_2 (±1%)	P_2O_5 (±1%)	density, g cm^{-3}	V_m, cm^3 mol^{-1}
P5	95	5	94.6	5.4	3.6353	29.30
P10	90	10	91.0	8.9	3.6268	29.88
P15	85	15	84.2	15.8	3.6139	30.50
P20	80	20	79.1	20.9	3.5976	31.16
P25	75	25	74.2	25.8	3.54	32.19

The slurry was heated overnight at 350 °C, a temperature high enough to dehydrate the batch but sufficiently low so as to avoid P_2O_5 loss, then melted at 1550 °C for 4 h and poured onto a steel plate to quench to glass. The bulk composition was checked with wet chemical analysis. This glass was then ground and mixed with the appropriate amounts of GeO_2 to give 50 g of each of the five compositions. These latter batches were melted at 1475−1500 °C in platinum crucibles for 2−3.5 h, and quenched to glass by air cooling. Exact compositions (from wet chemical analysis) are listed in Table 1, and for completeness, the sample densities are also given.

2.2. Nuclear Magnetic Resonance Spectroscopy. Phosphorus-31 magic angle spinning nuclear magnetic resonance spectroscopy (^{31}P MAS NMR) was performed on a Bruker Avance NMR spectrometer at a 283.49 MHz Larmor frequency (16.4 T magnet, 700 MHz proton frequency). The sample rotation frequency was 30 kHz, using 2.5 mm diameter rotors. Forty scans were acquired for each spectrum using a single pulse excitation of 2.25 μs following 60 s delays. The ^{31}P chemical shift scale was referenced against $NH_4H_2PO_4$ at 0.81 ppm. Natural abundance ^{17}O NMR spectra were also measured on the 700 MHz spectrometer at a Larmor frequency of 94.94 MHz with sample rotations of 12012 Hz in rotors of 4 mm diameter. A multiple RAPT (rotor-assisted population transfer) sequence[12] was followed by a Hahn echo and detection. In this experiment a series of RAPT pulses transfer polarization from the satellite transitions of quadrupolar nuclei to the central transition and thereby provide a significant enhancement in sensitivity over standard pulse excitation. Specifically, 21 Gaussian shaped pulse pairs of 18 μs duration and 30 kHz radio frequency field strength were used, spaced by 4 μs. These pulses were offset by amounts chosen to maximize signal for different magnitudes of quadrupole coupling. For example, ±540 kHz frequency offset was used for oxygen in sites resembling those in GeO_2 glass.[10] Following a *z*-filter of one rotor period duration the signal was detected with a Hahn echo using pulse lengths of 1.5 and 3.0 μs, respectively, and one rotor period spacing. Sixteen such experiments were performed in fast sequence without relaxation delay and saved in a 2-dimensional array. The spectra shown below are the center slices obtained after exponential multiplication and Fourier transformation in both dimensions. Over the course of 3.5 days 60 000 such experiments were added with 5 s recycle delays. The spectra are referenced to oxygen in tap water at 0 ppm.

2.3. Neutron Scattering. The neutron scattering data were obtained by using the Glass, Liquid and Amorphous Diffractometer (GLAD) on the Intense Pulsed Neutron Source, Argonne National Laboratory, Argonne, Illinois. Data reduction with the standard methodology available on GLAD[13] yielded the total correlation function $T(r)$ for each sample. By using the definition of the pair distribution function, $g_N(r)$, from Susman et al.[14]

$$g_N(r) = 1 + \frac{1}{4\pi\rho}\int_0^\infty [S_N(Q) - 1]\frac{Q^2 \sin Qr}{Qr}\,dQ \qquad (1)$$

and its relation to $T(r)$

$$T(r) = 4\pi\rho r g_N(r) \qquad (2)$$

the following is obtained:

$$T(r) = 4\pi\rho r + \int_0^\infty [S_N(Q) - 1]\sin Qr\,dQ \qquad (3)$$

where ρ is the atomic number density, $S_N(Q)$ the neutron structure factor, and Q the scattering vector. The expected slope, $4\pi\rho$ of $T(r)$ at large r, from eq 3, was calculated and compared to the experimental value as a useful check of the data quality. Note that alternative definitions of $g_N(r)$ give an extra factor of $2/\pi$ in eq 3.[15] Then, for each sample, Gaussian functions were fitted to the peaks in $T(r)$; we used Gaussians of the form

$$A\exp\left[\frac{-(r - r_0)^2}{2\sigma^2}\right] \qquad (4)$$

where A is the amplitude, r_0 is the peak center (which we identify with a bond length), and σ, the width, is related to the full width at half-maximum (fwhm) by $\sigma = \text{fwhm}/2\sqrt{2\ln 2}$. To obtain the coordination number c_{ij} of atoms j around atom i, $rT(r)$, which is related to the number density, is integrated over the peak assigned to $i-j$ interactions. Due to peak overlap, the integration is actually carried out by using the fitted Gaussian functions, as follows:

$$c_{ij} = \frac{\int_{r_1}^{r_2} rT(r)\,dr}{2w_{ij}} = \frac{Ar_0\sigma\sqrt{2\pi}}{2w_{ij}} \qquad (5)$$

The weighting factors account for concentrations c_i and neutron scattering length $\bar{b}_i$ through

$$w_{ij} = \frac{c_i\bar{b}_i c_j}{[\sum c_i\bar{b}_i]^2} \qquad (6)$$

Average coordination numbers only can be obtained. Appropriately weighted ratios of the integrals of $rT(r)$ yield the atomic fractions in different coordinations, for instance N_6, the fraction of 6-fold coordinated germanium atoms.

2.4. Glass Transition Temperatures and Viscosity Data. Glass transition temperatures were obtained by Corning Inc.,

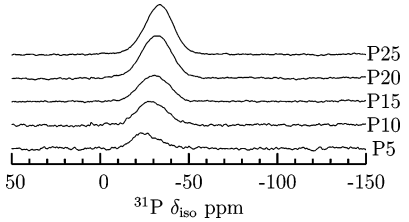

Figure 2. ^{31}P magic angle spinning NMR spectra of $GeO_2-P_2O_5$ glasses, as a function of mol % P_2O_5. P5 indicates 5 mol % P_2O_5, P10 indicates 10 mol % P_2O_5, and so forth. Larmor frequency: 283.49 MHz. Sample rotation frequency: 30 kHz. Reference: $NH_4H_2PO_4$ at 0.81 ppm.

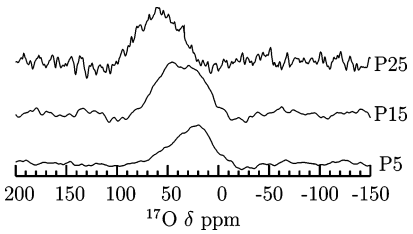

Figure 3. ^{17}O magic angle spinning NMR spectra of $GeO_2-P_2O_5$ glasses as a function of P_2O_5 content. The spectra were acquired at natural abundance ^{17}O content with the rotation assisted polarization transfer method (RAPT). P5: 5 mol % P_2O_5. P15: 15 mol % P_2O_5. P25: 25 mol % P_2O_5. Reference: water at 0 ppm.

USA, using differential thermal analysis (DTA). Measurements were performed in air, heating at 10 °C/min. Viscosity measurements were made by using the parallel plate technique for samples P5, P10, P15, and P25, and combined with the T_g data (assumed to correspond to a viscosity of 10^{13} P) to produce relevant plots for analysis.

2.5. First-Principles Calculations. NMR parameters of crystalline reference compounds were computed by using the NMR module[16,17] of the CASTEP code.[18] This code uses a density functional theory approach, implemented using a plane-wave basis and pseudopotentials to describe the atomic cores. Additionally it includes code to calculate the magnetic field response and the electric field gradient tensors. This method has been validated recently on a variety of oxide and glassy materials.[19] The calculations were performed by using ultrasoft pseudopotentials generated within the code from the proprietary "on-the-fly" method. Oxygen, phosphorus, and germanium were treated with valence spaces and cutoffs of respectively $2s^22p^6$ and 1.3 bohr, $3s^23p^5$ and 1.8 bohr, and $4s^24p^2$ and 2.1 bohr. The $L = 2$ state was used for the local potential in each case, and two projectors were used for the s and p pseudopotentials. All calculations used the experimental crystal structures. The revised PBE exchange-correlation functional was used,[20] and for integrations in reciprocal space, unshifted Monkhorst−Pack grids with spacings <0.04 Å^{-1} were used.[21] Wave functions were expanded in planewaves with a maximum energy of 610 eV, which we found sufficient to achieve convergence of the NMR parameters (isotropic chemical shift and quadrupole coupling) to the 1% level.

3. Results

^{31}P MAS NMR spectra are shown in Figure 2, as a function of P_2O_5 content. The spectra are offset vertically for clarity of presentation. Natural abundance ^{17}O MAS NMR spectra are shown in Figure 3. These spectra were obtained with conditions best suited for oxygen quadrupole couplings in the 7−8 MHz range; additional spectra optimized for 4.4 MHz couplings showed no additional spectra features. The neutron diffraction data are summarized in Figure 4, where only the total correlation functions are shown as a function of P_2O_5 content, again offset for clarity. Figure 5 summarizes the glass transition temperatures as a function of P_2O_5 content, and Figure 6 the viscosity. The viscosity data are represented in an Angell plot, where viscosity is plotted on a logarithmic scale as a function of inverse temperature scaled to the glass transition temperature of each sample. The results of the first-principles calculations, including isotropic chemical shift and quadrupole parameters where relevant, are listed in Table 2 for the different model compounds. The calculation actually provides chemical shielding, not shift; to convert to shifts and for ease of comparison with experiment, the ^{17}O shieldings are referenced to the calculated GeO_2 (quartz structure) value and the ^{31}P shieldings are referenced to the calculated P_2O_5 value.

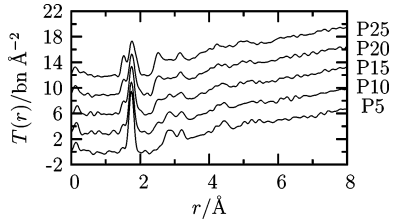

Figure 4. Total correlation functions $T(r)$ from neutron diffraction for $GeO_2-P_2O_5$ glasses as a function of mol % P_2O_5. P5 indicates 5 mol % P_2O_5 and so forth for the other labels.

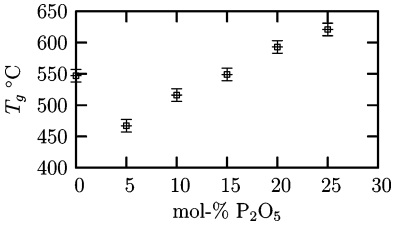

Figure 5. Glass transition temperature T_g measured by differential thermal analysis (in °C) of $GeO_2-P_2O_5$ glasses as a function of P_2O_5 content.

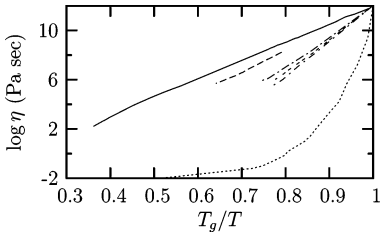

Figure 6. Viscosity of $GeO_2-P_2O_5$ liquids as a function of inverse temperature, scaled to their respective glass transition temperatures: solid line, GeO_2; single dashed line, P5; dash−dot line, P10; double-dash line, P15; short dash−dot line, P25. P5 means 5 mol % P_2O_5 and so forth. The dotted line gives $Ca(NO_3)_2-KNO_3$, a very fragile glass forming liquid included for comparison. The fragility is related to the slope of the curve at T_g; the liquids become more fragile as P_2O_5 is added.

4. Discussion

4.1. Crystalline Model Compounds. As a body of relevant crystalline compounds to which to compare the $GeO_2-P_2O_5$ glass system, we consider polymorphs of GeO_2, P_2O_5, and the two crystalline germanium phosphates found in the literature, germanium oxide hexakis(phosphate), $Ge_5O(PO_4)_6$,[22] and germanium diphosphate, GeP_2O_7.[23] The two forms of GeO_2 considered are the metastable quartz-like phase, in which each Ge atom is tetrahedrally coordinated to bridging oxygen and

TABLE 2: NMR Parameters for Oxygen and Phosphorus Sites Obtained from First-Principles Calculations[a]

compd	site	δ_{iso}/ ppm	C_Q/ MHz	η	δ^Q_{iso}/ ppm
GeO_2(quartz)	bridging ^{17}O	0.0	7.65	0.6	−53
GeO_2(rutile)	trigonal ^{17}O	106.1	8.20	0.08	−45
P_2O_5	bridging ^{17}O	31.7	8.8	0.25	−55
	capping ^{17}O	130.7	4.4	0.2	−13
	Q^3 ^{31}P	0.0			
$Ge_5O(PO_4)_6$	$Ge^{IV}-{}^{17}O-P$	22.0	7.6	0.2	−40
	$Ge^{IV}-{}^{17}O-Ge^{IV}$	48.0	6.6	0.5	−36
	$Ge^{VI}-{}^{17}O-P$	33.0 (long Ge−O)	7.5	0.25	−40
		−7 (short Ge−O)	8.2	0.4	−52
	Q^3 ^{31}P	23.0			
GeP_2O_7	$Ge^{VI}-{}^{17}O-P$	37.7	7.4	0.3	−40
	Q^3 ^{31}P	25.0			

[a] The chemical shift for ^{17}O is referenced to the calculated value in quartz GeO_2 at 0 ppm, and that of ^{31}P to the calculated value in P_2O_5 at 0 ppm. The final column gives the contribution of the quadrupole interaction in ^{17}O to the total shift in a 16.44 T magnet, as was used in the present experiments.

the tetrahedra are corner-sharing, see Figure 1a,e, and the rutile-structured phase, in which each Ge is octahedrally coordinated, see Figure 1b. In the rutile phase the oxygen atoms are 3-fold coordinate, such that along the crystal *c* axis there is a chain of edge-sharing Ge octahedra that are linked through corners in the *a*−*b* plane to neighboring chains. The P_2O_5 phase studied is orthorhombic, with each phosphorus atom tetrahedrally coordinated by four oxygens such that three are bridging and one is a double-bonded capping site, Figure 1c. The germanium oxide hexakis(phosphate) compound has the stoichiometry $(GeO_2)_5(P_2O_5)_3$, and thus has 37.5% P_2O_5. Its structure consists of a helix of GeO_6 octahedra, sharing faces connected through phosphate groups. The phosphates are similar to those found in P_2O_5 except that the formally double-bonded capping oxygen is also ligated to octahedral germanium atoms. Along the outer edges of the helix is an alternating pattern of terminating, corner-sharing tetrahedral germanium sites and bridging octahedral sites linking adjacent helices. The octahedral and tetrahedral germanium are present in a ratio of 3:2. The phosphorus atoms are all linked to three octahedral germanium second neighbors and one tetrahedral germanium second neighbor. Germanium diphosphate, GeP_2O_7, corresponds to the 1:1 $GeO_2-P_2O_5$ stoichiometry. In this compound all germanium atoms are octahedrally coordinated, and linked through phosphate corners to neighboring germanium sites. The phosphorus atoms are tetrahedrally coordinated by bridging oxygen, see Figure 1d, and each phosphorus has three germanium second neighbors and one phosphorus second neighbor.

4.2. ^{31}P MAS NMR. The spectra are shown in Figure 2. For all compositions, only one phosphorus contribution is apparent. The observed shift overlaps with that observed for Q^3 species in other phosphate glasses, and with that observed in $Ge_5O(PO_4)_6$,[24] and thus from the shift alone would be assigned as either Q^3 or Q^4 with asymmetric bonding. The shift values, extracted from fitting a single Gaussian to each spectrum, are summarized in Table 3. The proposed structures are consistent with the expected behavior that, because no modifying cations are present, no NBO atoms are formed. The spectra show a slight increase in width as phosphate content increases, and a more significant shift of 8 ppm toward increased shielding as P_2O_5 content rises from 5% to 25%. The computational results in Table 2 indicate that the ^{31}P shift in pure P_2O_5 is about 25 ppm more shielded than that of GeP_2O_7, in which each phosphate has three Ge^{VI} second neighbors and one phosphate second neighbor, and 23 ppm more shielded than in $Ge_5O(PO_4)_6$, in which each phosphate has three Ge^{VI} neighbors and one Ge^{IV}. Hence the increased shielding with P_2O_5 content observed in the glasses can be attributed to the increase in the number of phosphate neighbors. In P5 it is likely that almost all phosphate groups would have germanium polyhedra exclusively as neighbors; as P_2O_5 content increases, clearly the likelihood of phosphate second neighbors increases as well. The spectra are not well-enough resolved to quantify the second neighbor distribution as a function of P_2O_5 content. Nevertheless, a strong propensity for phosphate clustering can be ruled out, because in such a case the signal would be insensitive to further P_2O_5 addition.

TABLE 3: ^{31}P MAS and ^{17}O NMR Resonance Shifts in $GeO_2-P_2O_5$ Glasses as a Function of P_2O_5 Content[a]

sample	^{31}P shift (ppm)	^{17}O shift (ppm)
P5	−25.3	20
P10	−28.9	
P15	−30.3	40
P20	−31.7	
P25	−33.1	60

[a] Data referenced respectively for ^{31}P and ^{17}O to $NH_4H_2PO_4$ at 0.81 ppm and H_2O at 0 ppm.

4.3. ^{17}O Multiple RAPT NMR. The natural abundance ^{17}O MAS NMR spectra shown in Figure 3 show no resolution of multiple distinct oxygen sites but do show a clear progression from a peak center of about 20 ppm in the 5% P_2O_5 sample to about 60 ppm in the 25% P_2O_5 sample (Table 3). Because of the signficant quadrupole interactions to which ^{17}O is subject, interpreting this shift is more complex than in the ^{31}P case. In particular, the peak maximum position is subject to both the chemical shift and the isotropic component of the second-order quadrupole effect; the peak position is the sum of both terms. For precise work, peak positions from MAS spectra are not sufficient to determine these parameters, and more sophisticated experiments such as multiple-quantum MAS are required.[25] Under natural abundance conditions, however, such experiments are not feasible in general; perhaps more pertinent here is that the symmetry of the line shapes suggests that quadrupole effects are not overwhelming at the present field strength (as they would be in lower field) and so the present MAS spectra can be interpreted at least qualitatively with the aid of the first-principles calculations presented in Table 2.

First, the sample with 5% P_2O_5 content shows a total shift of 20 ppm (relative to water). Taking this shift to arise from $Ge^{IV}-O-Ge^{IV}$links, as in glassy GeO_2,[9] we then assess the trend toward more positive shifts with increasing P_2O_5 content in light of the computed shifts and quadrupole interactions for different sites. We thus consider sites in Table 2 that provide a total shift of about 40 ppm relative to the total shift computed for quartz-like GeO_2. Several of the sites listed in Table 2 appear immediately to be poor candidates to explain this shift, including the trigonal oxygen of rutile GeO_2 and the capping oxygen in P_2O_5. Both have total shifts much more positive than the trend observed. On the other hand, the computed total shift of $Ge^{IV}-{}^{17}O-P$ in $Ge_5O(PO_4)_6$ is 35 ppm relative to quartz-like GeO_2, close to the observed value. Other total shifts from the germanium phosphate samples are also roughly of the correct magnitude and cannot be rejected with high confidence based on these calculations. We can conclude, however, that oxygen sites of the trigonal, rutile form, and of the purely double-bonded capping type found in P_2O_5, are at most minor structural elements in these glasses. Instead, the oxygen data are most consistent with Q^4 phosphorus in which all four oxygens are

TABLE 4: Peak Locations and Assignments from the Total Neutron Correlation Functions $T(r)$ for $GeO_2-P_2O_5$ Glasses as a Function of Composition, and Derived Fraction of 6-Fold Coordinate Germanium N_6

	peak locations (Å) and assignments				
sample	P═O	P−O	G^{IV}	Ge^{VI}	N_6
P5	1.493 ± 0.003		1.744 ± 0.002		0
P10	1.462 ± 0.001	1.521 ± 0.002	1.746 ± 0.002	1.923 ± 0.018	0.022 ± 0.005
P15	1.475 ± 0.005	1.531 ± 0.004	1.750 ± 0.002	1.917 ± 0.012	0.030 ± 0.006
P20	1.467 ± 0.006	1.533 ± 0.002	1.755 ± 0.002	1.945 ± 0.018	0.033 ± 0.005
P25	1.476 ± 0.003	1.538 ± 0.002	1.758 ± 0.003	1.902 ± 0.006	0.102 ± 0.017

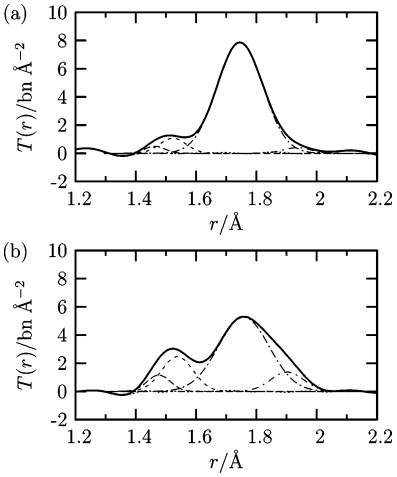

Figure 7. Gaussian peak fits to first neutron diffraction peaks for glass with (a) 10 and (b) 25 mol % P_2O_5.

shared with neighbors, most of which are Ge atoms. Note that the sharing is not equal—in $Ge_5O(PO_4)_6$, for example, the phosphorus atoms are four-coordinate, with each bonded oxygen linked to Ge sites; however, three of the P−O bonds are 1.51 Å while the fourth is 1.48 Å. Thus the latter site retains some but not all of the double-bond character found in pure P_2O_5.

4.4. Neutron Diffraction. The total correlation functions, $T(r)$, can be seen in Figure 4. Results from peak fitting are listed in Table 4, and Figure 7 shows example fits for samples P10 and P25. Although exposure to air was minimized, all glasses contain a small amount of water, on the order of 1%, as evidenced by the rise in $T(r)$ below $r \approx 0.5$ Å. This contamination does not interfere with peak analysis. The ^{31}P and ^{17}O NMR data together indicate asymmetric Q^4 bonding for the phosphorus tetrahedra, and this assignment is confirmed by the fits to the P−O bond lengths in the neutron total correlation functions (Table 4). Where multiple P−O peaks can be confidently fit, they show bond lengths of 1.48 and 1.53 Å, in good agreement with those in $Ge_5O(PO_4)_6$.[22] We thus assigned all phosphorus sites to asymmetric Q^4 species, with three long bonds and one short bond. This assignment was used to constrain the integrals $\int_{r_1}^{r_2} rT(r)\,dr$ of the P−O peaks in the ratio 3:1, for long P−O bonds compared to short P−O bonds. The feature in the correlation functions at about 1.75 Å is assigned to Ge−O correlations in GeO_4 tetrahedra, based both on its intensity and position. At compositions of 10 mol % P_2O_5 and above, an additional feature at about 1.9 Å appears, which is assigned to Ge−O correlations in GeO_6 species. It must be pointed out that for the lower P_2O_5 concentrations both the short P−O correlation and Ge^{VI}−O peaks are comparable to the noise level in $T(r)$. Errors are given accordingly. However, it was clear from the NMR results and the neutron peak fitting that these contributions must be present, and it has been possible to perform fits that yield reasonable parameter values, hence supporting this as a valid approach. For sample P5, no attempt was made to differentiate the phosphorus−oxygen contributions since the peak was simply too small. A single Gaussian, only, was fitted. Further, if any Ge^{VI} atoms are present in this glass, their concentration is negligible.

No definitive information could be obtained from the peaks at distances beyond the Ge−O correlations, as there are clearly numerous possible contributions at these ranges.

To check whether the structures suggested above are internally self-consistent, the atomic valences could be summed for each composition. Thus, assigning −2 to oxygen, +4 to Ge^{IV}, +6 to Ge^{VI}, +5 to Q^3, and +4 to fully bridged tetrahedral phosphorus, the total valence sum should be zero and thus constrains the proportions of the different units. In this simple approach, a structure consisting purely of Ge^{IV} and Q^3 for each composition satisfies the valence sum rule, but is clearly at odds with the neutron diffraction data. The presence of Ge^{VI}, as indicated by the neutron data, requires the presence of +4 phosphorus for charge balance; using the estimate for N_6 from Table 4 would be consistent with a mix of Q^3 and +4 phosphorus. As noted above the ^{17}O NMR data do not rule out a minor contribution of Q^3 sites. The limitation in this approach to checking structures is that the phosphorus sites probably are best described as asymmetric four-coordinate phosphorus, as we have done above, and hence are intermediate between Q^3 units with +5 valence and doubly bonded oxygen, and symmetrically bridged tetrahedral phosphorus with strictly +4 valence. Absent more detailed data, say from phosphorus photoelectron spectroscopy, the exact contributions of these sites to valence sums cannot be made in an informative way.

4.5. Viscosity and T_g Data. Initially, T_g drops in value upon addition of 5% P_2O_5 as compared to the value for vitreous GeO_2. The rise in T_g seen after 5 mol % P_2O_5, compared to pure vitreous GeO_2 (Figure 5), may be sensibly explained by the appearance of an increasing amount of 6-fold coordinated germanium atoms as the more highly bonded GeO_6 octahedra result in a greater network connectivity. On the other hand, however, this would appear to contradict the glass fragility displayed in the Angell diagram, Figure 6, since a higher degree of fragility is typically associated with a lower degree of short-range structural order, and the data here imply that germanophosphate liquids become more fragile as P_2O_5 is added to the matrix and germanium octahedra are formed.

This apparent discrepancy may in fact be due to differing structural elements dominating T_g and fragility. Novikov and Sokolov recently showed a striking correlation between the Poisson ratio in the glass and the fragility of the associated melt;[26] the correlation set included a number of inorganic oxide glasses. They concluded that the loss of shear strength correlates closely with increased fragility. In the present case, it may be that the increase in GeO_6 octahedra contributes to such a decrease in shear modulus. The reason lies in the fact that octahedra are over-coordinated with respect to filling space efficiently when linked through corner-sharing oxygen. This conclusion has been reached by various constraint counting models of glass formation.[27−29] Therefore, it may well be that

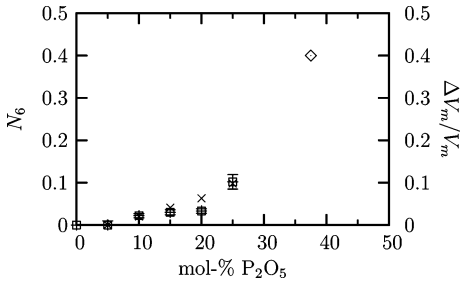

Figure 8. Fraction of 6-fold coordinate Ge in $GeO_2-P_2O_5$ glasses (squares, with error bars) as a function of mol % P_2O_5 content, based on fits to neutron diffraction data constrained by NMR results. The diamond represents the N_6 value for crystalline $Ge_5O(PO_4)_6$. Plotted with ×'s on the right axis is the fractional change in molar volume, relative to the P5 sample (5 mol % P_2O_5 content).

some of the octahedra that do form link otherwise compact domains, much as is seen in $Ge_5O(PO_4)_6$. There, the helical structures are linked by GeO_6 octahedra spaced at intervals of a half-turn of the helix; the result is a structure with a noticeable fraction of void space.[22] We would suggest then that in order to incorporate the octahedra, the glasses must develop a somewhat looser structure to accommodate the over-coordination. Such a structure should be reflected in the molar volume (Table 1); in Figure 8 we plot the fractional change in molar volume $\Delta V_m/V_m$ as a function of composition, referenced to the P5 sample. The change in this parameter-free quantity tracks very closely the trend in the generation of germanium octahedra, suggesting that indeed the incorporation of the GeO_6 octahedra results in a significant loosening of the structure. Ultimately, the looser structure required by the formation of the octahedra would likely decrease the shear modulus, resulting in an increase in fragility, as observed.

4.6. Comparison with the $GeS_2-P_2S_5$ System. $GeS_2-P_2S_5$ glasses differ from $GeO_2-P_2O_5$ in two major respects. First, while $GeO_2-P_2O_5$ shows formation of Ge^{VI} at higher P_2O_5 content, in $GeS_2-P_2S_5$ the coordination number of Ge is always four.[6,7] On the other hand, in $GeO_2-P_2O_5$ phosphorus is found exclusively in the four-coordinate P^V state, while in $GeS_2-P_2S_5$ there is a complex mixture of P^{III} and P^V, with formation of $-S-S-$ bonds (that is, S^0) to balance the reduced P^{III}. Because sulfur is somewhat more electronegative than phosphorus (2.6 vs 2.2 on the Pauling scale) we had expected no reduction of phosphorus in the $GeS_2-P_2S_5$ glasses. Evidently, that difference was not enough to maintain phosphorus in the fully oxidized state. Here, though, in $GeO_2-P_2O_5$ glasses the very large electronegativity difference between O and P (3.4 vs 2.2) is enough to maintain simple oxidation states for all elements.

5. Conclusions

The structure of $GeO_2-P_2O_5$ glasses consists of GeO_4 tetrahedra at low P_2O_5 content, with an increasing fraction of GeO_6 units with increasing P_2O_5 content. The fraction of GeO_6 units, N_6, appears to follow a trend directly toward its value in crystalline $Ge_5O(PO_4)_6$. We detected no signature of trigonal oxygen, indicating that even in the presence of GeO_6 units the glasses do not resemble rutile-structured GeO_2, a finding again in accord with the structure of $Ge_5O(PO_4)_6$. The phosphate units are all four-coordinate, but unlike in P_2O_5 the formally double-bonded capping oxygen is shared asymmetrically with neighboring Ge sites, as in $Ge_5O(PO_4)_6$ and GeP_2O_7.

The glass transition temperature of $GeO_2-P_2O_5$ shows a distinct initial decrease from its value in GeO_2 to that at 5% P_2O_5 content, followed by a gradual increase; this behavior does not correlate with the formation of GeO_6 species and so suggests a different origin from so-called germanate anomalies in alkali germanates. At the same time, the viscosities indicate increasing fragility with P_2O_5 content. The increase in glass transition temperature is due to the overall increase in connectivity, while the increase in fragility is ascribed to a likely decrease in shear modulus, brought on by the requirement of incorporating the over-coordinated germanium octahedra in the amorphous network. Such an incorporation would require a looser structure and an increase in molar volume, the extent of which was found experimentally to match closely the increase in octahedral germanium.

References and Notes

(1) Fu, J. *Solid State Ionics* **1997**, *104*, 191.

(2) Sakaguchi, S.; Todoroki, S.; Rigout, N. *J. Non-Cryst. Solids* **1996**, *196*, 58.

(3) Shimizugawa, Y.; Marumo, F.; Nukui, A.; Ohsumi, K. *J. Non-Cryst. Solids* **1994**, *176*, 76.

(4) Weeding, T. L.; de Jong, B. H. W. S.; Weeman, W. S.; Aitken, B. G. *Nature* **1985**, *318*, 352.

(5) Müller, D.; Berger, G.; Grunze, I.; Ladwig, G.; Hallas, E.; Haubenreiser, U. *Phys. Chem. Glasses* **1983**, *24*, 37.

(6) Cherry, B.; Zwanziger, J. W.; Aitken, B. G. *J. Phys. Chem. B* **2002**, *106*, 11093−11101.

(7) Cherry, B.; Zwanziger, J. W.; Aitken, B. G. *J. Non-Cryst. Solids* **2004**, *333*, 28−36.

(8) Khan, M. H. *J. Mater. Sci. Lett.* **1986**, *5*, 685−686.

(9) Stone, C. E.; Hannon, A. C.; Ishihara, T.; Kitamura, N.; Shirakawa, Y.; Sinclair, R. N.; Umesaki, N.; Wright, A. C. *J. Non-Cryst. Solids* **2001**, *293−295*, 769−775.

(10) Hussin, R.; Holland, D.; Dupree, R. *J. Non-Cryst. Solids* **1998**, *232−234*, 440−445.

(11) Dupree, R.; Holland, D.; Mortuza, M. G. *Nature* **1987**, *328*, 416−417.

(12) Kwak, H.-T.; Prasad, S.; Clark, T.; Grandinetti, P. J. *Solid State NMR* **2003**, *24*, 71−77.

(13) Ellison, A. J. G.; Crawford, R. K.; Montague, D. G.; Volin, K. J.; Price, D. L. *J. Neutron Res.* **1993**, *1*, 61−70.

(14) Susman, S.; Volin, K. J.; Price, D. L.; Grimsditch, M.; Rino, J. P.; Kalia, R. K.; Vashista, P.; Gwanmesia, G.; Wang, Y.; Liebermann, R. C. *Phys. Rev. B* **1991**, *43*, 1194.

(15) Wilding, M. C.; Benmore, C. J.; Tangeman, J. A.; Sampath, S. *Europhys. Lett.* **2004**, *67*, 212−218.

(16) Pickard, C. J.; Mauri, F. *Phys. Rev. B* **2001**, *63*, DOI 245101.

(17) Profeta, M.; Mauri, F.; Pickard, C. J. *J. Am. Chem. Soc.* **2003**, *125*, 541.

(18) Segall, M. D.; Lindan, P. J. D.; Probert, M. J.; Pickard, C. J.; Hasnip, P. J.; Clark, S. J.; Payne, M. C. *J. Phys.: Condens. Matter* **2002**, *14*, 2717−2743.

(19) Charpentier, T.; Ispas, S.; Profeta, M.; Mauri, F.; Pickard, C. *J. Phys. Chem. B* **2004**, *108*, 4147−4161.

(20) Hammer, B.; Hansen, L. B.; Norskov, J. K. *Phys. Rev. B* **1999**, *59*, 7413−7421.

(21) Monkhorst, H. J.; Pack, J. D. *Phys. Rev. B* **1976**, *13*, 5188−5192.

(22) Mayer, H.; Völlenkle, H. *Monatsh. Chem.* **1972**, *103*, 1560−1571.

(23) Kaiser, U.; Glaum, R. Z. *Anorg. Allg. Chem.* **1994**, *610*, 1755−1759.

(24) Losilla, E. R.; Cabeza, A.; Bruque, S.; Aranda, M. A. G.; Sanz, J.; Iglesias, J. E. *J. Solid State Chem.* **2001**, *156*, 213−219.

(25) Brown, S. P.; Wimperis, S. *J. Magn. Reson.* **1997**, *42*, 42−61.

(26) Novikov, V. N.; Sokolov, A. P. *Nature* **2004**, *431*, 961−963.

(27) Gupta, P. K.; Cooper, A. R. *J. Non-Cryst. Solids* **1990**, *123*, 14−21.

(28) Thorpe, M. *J. Non-Cryst. Solids* **1983**, *57*, 355.

(29) Phillips, J. *J. Non-Cryst. Solids* **1979**, *34*, 153.